Received: 28 October 2022 | Revised: 11 May 2023 | Accepted: 11 July 2023

DOI: 10.1002/qua.27208

RESEARCH ARTICLE

International Journal of Quantum Chemistry WILEY

Organic light-emitting diode behaviors of some synthesized platinum(II)-based complexes

Ayhan Üngördü

Department of Chemistry, Faculty of Science, Sivas Cumhuriyet University, Sivas, Turkey

Correspondence
Ayhan Üngördü, Department of Chemistry, Faculty of Science, Sivas Cumhuriyet University, 58140, Sivas, Turkey.
Email: aungordu@cumhuriyet.edu.tr

Funding information
Sivas Cumhuriyet Üniversitesi

Abstract

Organic light-emitting light diodes (OLEDs) have been increasingly used in displays, replacing liquid-crystal displays (LCD) and light-emitting diodes (LEDs) panels. The increase in commercial use of OLED has led to the search for OLED with high performance. For that reason, the OLED properties of monomers and dimers of some synthesized platinum(II)-based complexes were estimated by using different computational chemistry tools with different codes. The electron/hole reorganization energies, the adiabatic/vertical ionization potentials, the adiabatic/vertical electron affinities, the chemical hardness values, the dipole moments, the frontier orbital shapes/energy levels, the energy gaps, the emission wavelengths, spin-orbit matrix elements, the rates of reverse intersystem crossing and intersystem crossing of the investigated complexes were determined. From the theoretically obtained data, it was found that $Pt(hppz)_2$ and $Pt(fppz)_2$ complexes can be used as electron transfer material. Furthermore, it was stated that Pt(f2bipz)(bpy) is both electron-blocking layer and hole blocking layer materials. Moreover, it was noted that that PtOEP complex can be utilized as a good electron injection layer and hole injection layer material. Addition to these, it was emphasized that that Pt(f2bipz)(bpy) can be considered as a good candidate for near infrared organic light emitting diodes and thermal activated delayed fluorescent organic light emitting diodes. In light of computational chemistry, it should be expected that the study will provide a great contribution to studies related to organic light emitting diodes.

KEYWORDS
charge transfer, DFT, Marcus theory, OLED materials, platinum(II) complexes

1 | INTRODUCTION

Since the first organic electroluminescence (EL) from tris-(8-hydroxyquinoline) aluminum (Alq3) has been discovered by Tang and Van Slyke [1], a lot of work has been made to develop the performance of organic light-emitting diode (OLED) devices [2–10]. Particularly, advances in device engineering technology have opened up a great deal of space for OLEDs in small and large panel manufacturing [11–15]. While large sized-OLED panels are used for high-performance displays such as television screens, computer monitors, signages, and so on, whereas small-sized-OLED panels are preferred for screens like smartphones, smartwatches, and handheld game consoles [16–23]. Compared with other display

technologies, OLEDs have some advantages because of their economical, flexible, bendable, foldable, transparent, and so on [24–28]. For that reason, it is hoped that OLEDs will take an important place in the display market in the future [29–32].

Multilayer OLED devices consist of anode–cathode electrodes and several organic layers (or organometallic layers) added between them, including the electron injection layer (EIL), the electron transfer layer (ETL), the hole blocking layer (HBL), the light emitting layer (LEL), the electron blocking layer (EBL), the hole transfer layer (HTL), the hole injection layer (HIL) [33–35]. All mentioned layers effect the performance of the OLED device [36]. Among them, the emissive layers play a dominant role in deciding the OLED performance, such and efficiency and color [37]. There are three kinds of light-emitting layers for OLED, namely fluorescent, phosphorescent, and thermal-activated delayed fluorescent (TADF) materials [38–40]. Fluorescent materials are primarily utilized in OLEDs [41]. However, the efficiency of first-generation OLEDs with fluorescent compounds is quite low [42]. The fluorescents can convert only 25% of excitons generated by electronic excitation to light because spin statistics determines that single and triplet excitons formed under electronic excitation are in a ratio of 1:3 [43]. This implies that the internal quantum efficiency (IQE) of the fluorescent OLEDs is capped at 25% [44]. For that reason, with the discovery of second-generation OLEDs called phosphorescent OLEDs (PhOLEDs) that utilized triplet excitons for light emission through intersystem crossing (ISC), the IQEs of green and red PhOLEDs have increased dramatically up to 100% [45, 46]. Nevertheless, blue PhOLEDs have been found to be not stable enough for industrial applications [47]. In this instance, the third-generation of the OLED materials that called TADF OLEDs have recently emerged [48]. By TADF materials, as in PhOLEDs, an internal quantum of efficiency of 100% is achievable because all excitons can be converted to light [49]. In addition, TADF OLEDs promise a longer device lifetime [50]. The TADF process can occur if the energy gap (ΔE_{ST}) between the first singlet (S_1) and the first triplet excited states (T_1) is low enough (<.2 eV) [51–53]. The small ΔE_{ST} facilitates reverse inter-system crossing (RISC) where triplet excitons may be up-converted to singlet excitons and radiate back to the ground state (S_0) via delayed fluorescence [54]. The aforementioned emission mechanisms used in the three generations of OLEDs are depicted in Scheme 1.

Even after the OLED developments mentioned above, the emergence of different types of OLEDs has continued [55–58]. For example, recently reported near-infrared (NIR) OLEDs that have emission peak wavelengths beyond 700 nm have used in important applications such as optical signal processing, commutation networks, night-vision devices, sensors, portable thermal imaging camera, photodynamic therapy, bioimaging, photopolymerization, and military systems used for defense [59–63]. In spite of the great potential for applications, the improvement of high-performance NIR OLEDs is hampered by strong nonradiative procedures as regulated by the energy gap law [64]. This law states that owing to the vibrational couplings and the vibrational overlaps existing between lowest excited singlet or triplet states and the ground state, nonradiative deactivation pathways can occur, and these nonradiative processes are greatly enhanced for compounds having small energy gaps [65]. Therefore, it can be stated that NIR emissive materials possessing small energy gap are excellent candidates for many intrinsic quenching mechanisms [66].

Basically, to eliminate this quenching process, the aforementioned vibrational overlap must be reduced [67]. For that reason, perfluorinated or perdeuterated approaches are utilized to reduce the number of high-frequency X–H vibrations (where X = C, N, or O) [68]. Nevertheless, the procedure mentioned is synthetically difficult and not also cost-effective [69, 70]. In addition, the aforementioned approach give rise to only partial or even insignificant improvements [71]. Alternatively, the high-frequency vibrational quenching can be theoretically importantly eliminated if the transition to the ground-state has a shallow and/or repulsive potential energy surface (PES), which describes the energy of a system, in the ground state [72]. The formation of the mentioned PES can be achieved by the creation of an excimer [73]. In this case, a way to surpass the energy gap law is provided [74].

On the other hand, platinum(II) transition-metal complexes having extended π-conjugation can be used as a key to induce the π-π stacking interactions between square-plane dimers to obtain longer wavelength emissions [75]. The lowest energy excited state of the platinum(II) compounds are generally characterized by a metal-to-ligand-charge transfer (MLCT) and/or ligand-to-ligand-charge transfer (LLCT) as well as ligand-centered (LC) triplet character in many examples [76]. Especially, the MLCT transition character meets the needs for shallow or repulsive PES in the ground state [77, 78].

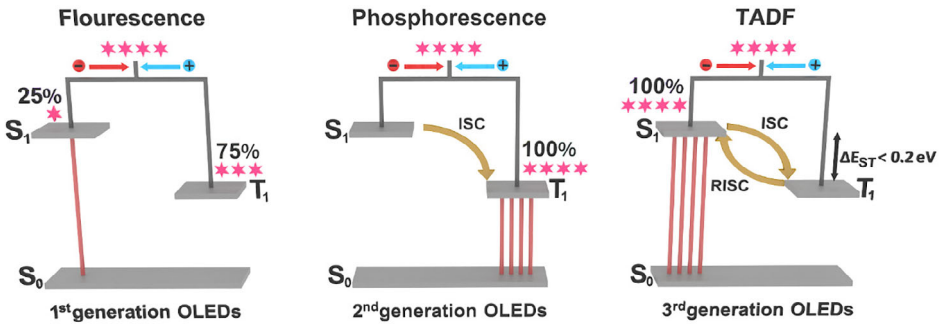

SCHEME 1 Schematic energy diagram for emission of the fluorescent, phosphorescent, and TADF OLED materials.

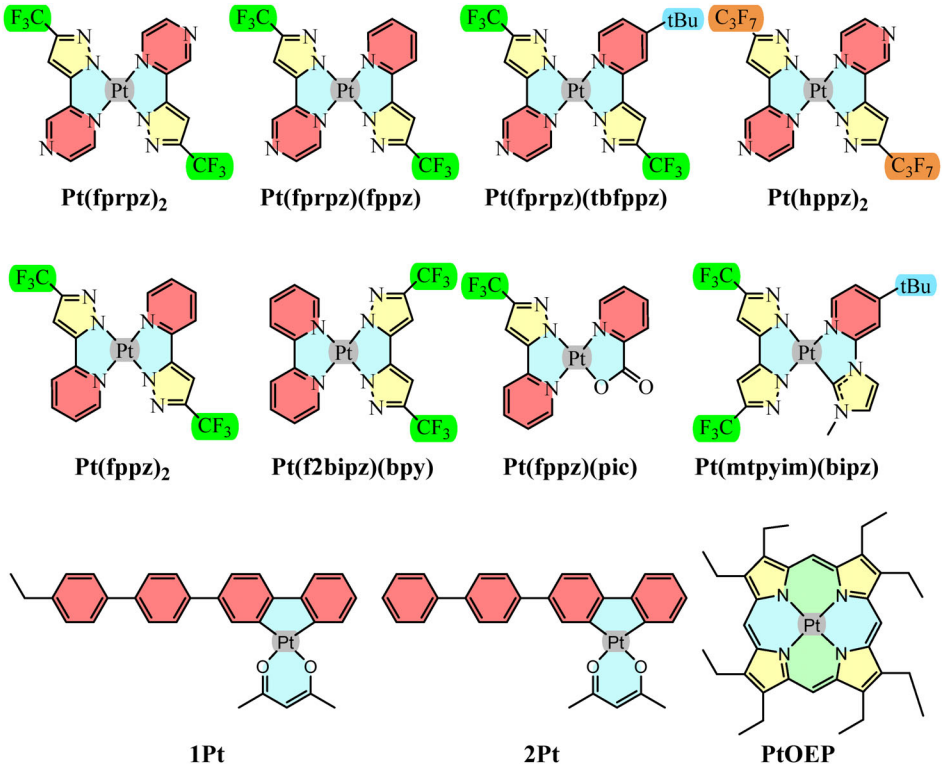

SCHEME 2 Molecular structures of the investigated Pt-based complexes [61, 79].

In this article, inspired by the above-mentioned studies, the OLED behaviors of some platinum(II)-based compounds given in Scheme 2 are predicted by computational chemistry tools with different codes. The OLED parameters of the studied Pt(II)-complexes are determined using density functional theory (DFT) method within different computational chemistry software packages. From the theoretically achieved results, it is hoped that suitable Pt(II)-compounds for OLED designs will be found.

2 | METHODS

All calculations were carried out by different computational software in the gas phase. Monomer calculations of the mentioned platin-based complexes were performed in Gaussian 16 [80], Amsterdam Density Functional (ADF) 2019 [81], and Schrödinger Suite 2021-2 [82] programs, respectively.

More than one code had to be used in the article. B3LYP hybrid functional of DFT was preferred because that is a good function for calculations of conjugated systems [83]. However, PBE0 hybrid functional of DFT for calculations involving emission calculations was used because the PBE0 functional gives good results in emission computations [84].

In some theoretical studies related to OLED materials, it is preferred the 6-31G(d) basis set. Because the 6-31G basis set takes into account all the electrons of the system. In this study, the 6-31G(d) basis set was used for atoms excluding the platinum element. In the calculations of Pt metals which are third-row transition metals, it cannot used aforementioned basis set. LANL2DZ basis set only takes into account valence and core electrons of the system. For that reason, it can be selected for large atoms. Furthermore, LANL2DZ is a good and safe choice for calculating properties based on valence electrons (as ionization energy, electron affinity, and reorganization energy…). Therefore, LANL2DZ basis set had to be selected for Pt metal. In other words, 6-31G(d) + LANL2DZ mixed basis set was used for performed calculations in Gaussian program such as the electron/hole reorganization energies, the adiabatic/vertical ionization potentials, the adiabatic/vertical electron affinities, the chemical hardness values, the dipole moments, the lowest unoccupied molecular orbital (LUMO) energy levels, the highest occupied molecular orbital (HOMO) energy levels and energy gaps.

On the other hand, there are not 6-31G(d) and LANL2DZ basis sets in Amsterdam Density Functional program. Instead of this mixed basis set, TZP basis set which is good basis set was preferred in ADF program because the TZP basis set can be used for all atoms in the examined complexes. In ADF program, the energies of the complexes in singlet ground, first singlet excited, and first triplet excited states were

computed at PBE0/TZP level. From the obtained data, the emission values and TADF parameters of the investigated Pt(II)-complexes were calculated.

Similar to ADF program, MIDIXL basis set was selected in Schrödinger program. MIDIXL basis set is a new basis set and it can be applied for all atoms such as TZP. In Schrödinger program, the reorganization energies, absorption/emission values, TADF parameters and dipole moments of the aforementioned monomers were calculated at B3LYP/MIDIXL level by using optimized structures obtained at B3LYP/6-31G(d)-LANL2DZ (Pt) level in Gaussian program.

It is required to note that the computational cost of dimer molecules in both Gaussian and ADF programs is quite high. Therefore, dimer compounds were optimized by using PBE0 functional with 6-31G(d)/LANL2DZ(Pt) basis sets in Gaussian program. After that, the reorganization energies, absorption/emission values, TADF parameters and dipole moments of the mentioned dimers were determined at B3LYP/MIDIXL level in Schrödinger program using the optimized geometries of the dimers. In this way, the computational cost of dimer complexes was greatly reduced.

Charge transfer rate (k) can be calculated by Marcus theory via the following equation [85]:

$$k = \frac{4\pi^2}{h} V^2 \frac{\exp(-\lambda/4k_B T)}{\sqrt{4\pi\lambda k_B T}}, \tag{1}$$

where V is the charge transfer integral, T is the absolute temperature, and λ is the sum of internal reorganization energy (λ_{int}) and external (λ_{ext}) reorganization energy. In addition to these parameters, k_B and h are the Boltzmann and Planck constants, respectively. The charge-transfer rate is determined by two key parameters, which are V and λ, at a certain temperature. To examine V, crystal data is usually needed. Nevertheless, the designed compounds can be noncrystal, and the charge transfer integral is very limited. For that reason, to explain the charge transfer rates of the studied complexes, their reorganization energies were taken into account. The reorganization energies are usually determined by a rapid change in molecular geometry when a charge is removed or added from compound (λ_{int}) and indicates the impact of the enraptured medium on charge transfer (λ_{ext}). The λ_{ext} was ignored in the previous studies because there is an obvious correlation between λ_{int} and charge transfer rates. Therefore, it was focused on the debate of the λ_{int} to explain the charge transfer rates of the investigated Pt(II)-complexes in this paper.

The reorganization energies (λs), the adiabatic/vertical ionization potentials (IPs), and the adiabatic/vertical electron affinities (EAs) can be calculated from single point energies via Equations 2–7: [86–88]

$$\lambda_e = \left(E_0^- - E_-^-\right) + \left(E_-^0 - E_0^0\right), \tag{2}$$

$$\lambda_h = \left(E_0^+ - E_+^+\right) + \left(E_+^0 - E_0^0\right), \tag{3}$$

$$IPa = E_+^+ - E_0^0, \tag{4}$$

$$IPv = E_0^+ - E_0^0, \tag{5}$$

$$EAa = E_0^0 - E_-^-, \tag{6}$$

$$EAv = E_0^0 - E_0^-, \tag{7}$$

where $E_0^-\left(E_0^+\right)$ presents the energy of the anion (cation) obtained through the optimized neutral complex. Likewise, $E_-^-\left(E_+^+\right)$ stands for the energy of the anion (cation) calculated using the optimized anion (cation) structure, $E_-^0\left(E_+^0\right)$ defines the energy of the neutral compound computed at the anionic (cationic) state. E_0^0 also states the energy of the neutral molecule at the ground state.

In addition to the aforementioned parameters, to estimate the stability of molecules, the absolute chemical hardness (η) [89] may be found by the adiabatic ionization potential (IPa) and the electron affinity (EAa) by Equation 8:

$$\eta = (IPa - EAa)/2. \tag{8}$$

The investigated complexes are both closed and open-shell systems. The emission calculation of the open-shell systems is harder than that of closed-shell systems. However, the emission values closed- or open-shell systems can be predicted by utilizing the energy differences between ground-state energy (E_0) and the lowest excited-state energies (E_1) of the compounds via Equations 9 and 10.

$$\Delta E = E_1 - E_0 \tag{9}$$

$$\lambda = \mathrm{hc}/\Delta E \tag{10}$$

wherein ΔE and λ presents the emission energy and wavelength, respectively. c shows the light speed and h states Planck constant.

Thermal activated delayed fluorescent (TADF) performance of compounds can be predicted by means of Equation 11 [90]:

$$\Delta E_{ST} = (ES_1 - ET_1). \tag{11}$$

Here, ES_1 is the lowest-energy excited singlet state, while ET_1 is the lowest-energy excited triplet state. Additionally, TADF involves a reverse intersystem crossing (RISC) process, in which S_1 states are populated from T_1 levels. RISC competes with other processes such as the $S_1 \rightarrow T_1$ intersystem crossing (ISC). However, if non-radiative paths are negligible, k_{RISC} represents the rate-determining factor for TADF.

The rate of reverse intersystem crossing (k_{RISC}) and the rate of intersystem crossing (k_{ISC}) and between S_1 and T_1 are calculated according to the Fermi Gulden rule [91, 92] given by Equations 12 and 13:

$$k_{RISC} = \frac{2\pi}{\hbar}\left|\left\langle S_1\middle|\widehat{H}_{SO}\middle|T_1\right\rangle\right|^2 \rho_{FCWD}, \tag{12}$$

$$k_{ISC} = 3k_{RISC}\left[\exp\left(\frac{-\Delta E_{ST}}{k_B T}\right)\right]^{-1}, \tag{13}$$

where $\left\langle S_1\middle|\widehat{H}_{SO}\middle|T_1\right\rangle$ is the spin-orbit coupling matrix element (SOCME) between S_1 and T_1 states and ρ_{FCWD} stands for the Franck-Condon-weighted density of states. While $\left\langle S_1\middle|\widehat{H}_{SO}\middle|T_1\right\rangle$ can be interpreted as probability for the $T_1 \rightarrow S_1$ transition, ρ_{FCWD} describes the thermokinetic barrier associated with this process. Classical Marcus theory (CMT) provides a simple way to describe this thermokinetic barrier. ρ_{FCWD}^{CMT} can be expressed with Equation 14:

$$\rho_{FCWD}^{CMT} = \frac{1}{\sqrt{4\pi\lambda_M k_B T}}\exp\left(-\frac{(\Delta E_{ST} + \lambda_M)^2}{4\lambda_M k_B T}\right). \tag{14}$$

Here, λ_M the Marcus reorganization energy [93] related with the intramolecular low-frequency vibrations and it can be calculated by the formula given in Equation 14:

$$\lambda_M = E_{S1/T1} - E_{S1/S1}, \tag{15}$$

where $E_{S1/S1}$ and $E_{S1/T1}$ are the excited states energies of optimized S_1 and T_1 structures, respectively.

3 | RESULTS AND DISCUSSION

3.1 | Monomers

All Pt(II)-complexes are optimized at B3LYP/6-31G(d)-LANL2DZ(Pt) level. The structures of the optimized complexes are shown in Figure 1. All of the Pt(II)-complexes given in Figure 1. are closed-shell systems, except for 1Pt and 2Pt complexes. In other words, the 1Pt and 2Pt compounds are open-shell systems with single electron numbers.

3.1.1 | Frontier molecular orbitals and band gaps

The energy gap (Egap) values and the frontier molecular orbitals (FMOs), which are the highest occupied molecular orbital (HOMO) and the lowest unoccupied molecular orbital (LUMO) shapes, of these optimized compounds are also obtained at the B3LYP/6-31G(d)-LANL2DZ(Pt) level. The acquired HOMO, LUMO shapes and energy gaps are presented in Figure 2.

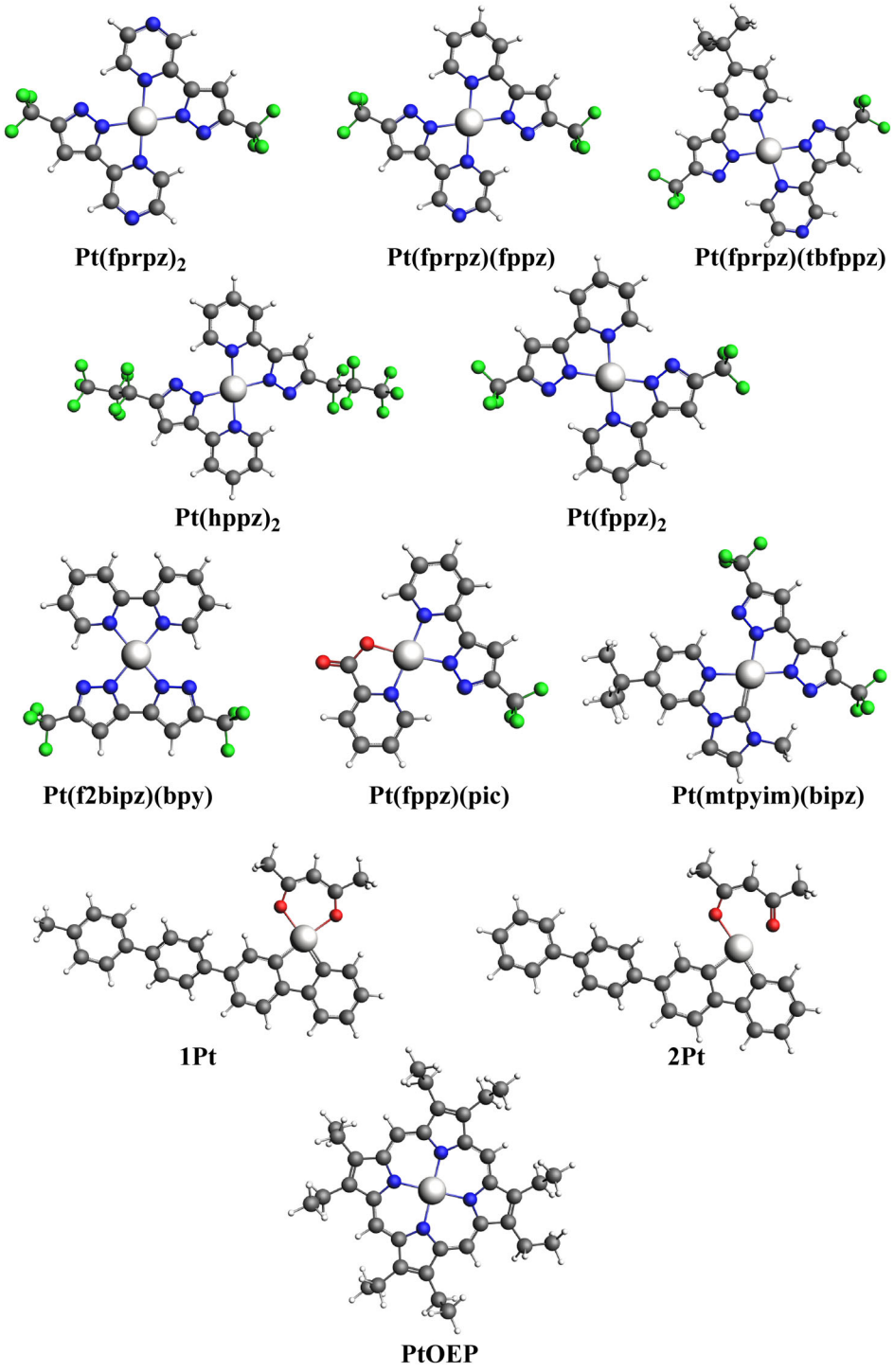

FIGURE 1 The optimized structures of the investigated Pt(II) monomers.

The interpretation of frontier molecular orbital shapes is useful for understanding electron transfer within molecular devices. One can see from Figure 2 that frontier molecular orbitals are delocalized on almost all molecules except for Pt(f2bipz)(bpy) and Pt(mtpyim)(bipz) complexes. The clear spatial separation of the FMOs of the Pt(f2bipz)(bpy) and Pt(mtpyim)(bipz) molecules causes to the obtaining of a small ΔE_{ST} as well as the occurrence of the intra-molecular charge transfer (ICT) process. Small ΔE_{ST} value implies a more effective TADF material. For that reason, it should be stated that Pt(f2bipz)(bpy) and Pt(mtpyim)(bipz) can be considered as suitable candidates for TADF OLED material. Additionally, it is widely reported that the Egap values are related to the optical and electronic properties [94]. From Figure 2, it is noticed that the electronic transition with the lowest energy among the investigated closed-shell system occurs in Pt(fppz)(pic) and Pt(mtpyim)(bipz) complexes. Among the closed-shell complexes, Pt(fppz)(pic) and Pt(mtpyim)(bipz) compounds exhibit high conductivity. Additionally, it can be said that the Egap values of compounds with open-shell systems are smaller than those of closed-shell complexes. Therefore, the conductivity is higher in the compounds

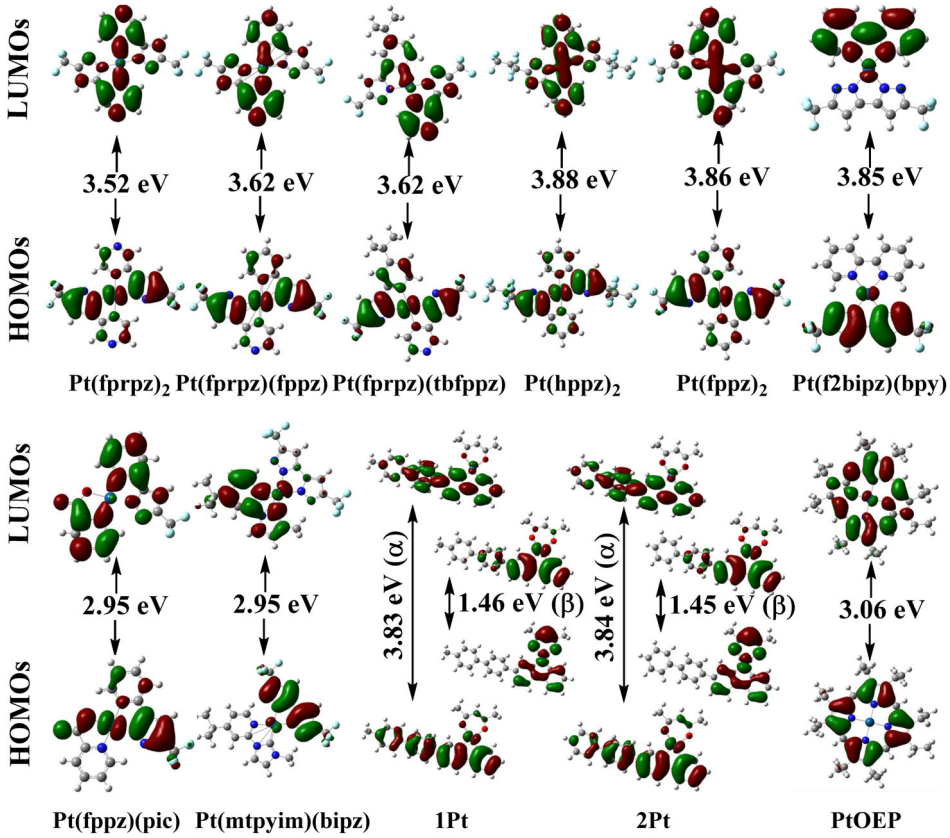

FIGURE 2 Energy gaps and frontier orbital shapes of the investigated complexes.

TABLE 1 The obtained computational chemical parameters (in eV) of the studied Pt(II)-monomers at hybrid B3LYP with 6-31G(d) and LANL2DZ(Pt) basis sets.

Complex	HOMO	LUMO	λe	λh	IPa	IPv	EAa	EAv	η	Dipole[a]
$Pt(fprpz)_2$	−6.52	−3.00	.22	.32	7.77	7.92	1.73	1.62	3.02	.00
Pt(fprpz)(fppz)	−6.31	−2.69	.22	.31	7.56	7.71	1.40	1.29	3.09	3.11
Pt(fprpz)(tbfppz)	−6.22	−2.60	.23	.31	7.44	7.58	1.33	1.21	3.06	4.46
$Pt(hppz)_2$	−6.17	−2.30	.18	.32	7.37	7.52	1.08	.99	3.15	.00
$Pt(fppz)_2$	−6.11	−2.25	.18	.31	7.36	7.50	1.00	.91	3.18	.00
Pt(f2bipz)(bpy)	−5.38	−3.07	.39	.62	6.63	6.94	1.79	1.59	2.43	13.79
Pt(fppz)(pic)	−6.15	−2.29	.21	.43	7.48	7.68	1.00	.89	3.24	2.28
Pt(mtpyim)(bipz)	−5.21	−2.26	.32	.63	6.44	6.75	1.02	.86	2.71	15.49
1Pt	−5.46 (α) −5.52 (β)	−1.63 (α) −4.06 (β)	.22	.32	6.48	6.64	2.84	2.73	1.82	2.49
2Pt	−5.50 (α) −5.54 (β)	−1.66 (α) −4.09 (β)	.22	.32	6.54	6.71	2.85	2.74	1.85	1.95
PtOEP	−4.92	−1.86	.23	.36	6.01	6.32	.94	.67	2.54	.28

[a]The unit of dipole moment is Debye.

with the open shell system compared with the complexes with the closed shell system. As a result, the compounds with the lower Egap value can be preferred for OLEDs in the field of optoelectronics.

On the other hand, it has been reported that the frontier molecular orbital energy levels of molecules play an important role in OLED performance [95]. According to the report, higher exciton recombination occurs when the energy barrier between OLED layers is lower than .4 eV. The LUMO levels of the molecules in the layer play a more important role than its HOMO levels in the governance of exciton recombination. Accordingly,

to obtain high-performance OLEDs, especially the differences between the LUMO values of the compounds located next to each other in the OLED layers should be taken into account. The HOMO and LUMO energy levels of the investigated complexes are calculated at B3LYP/6-31G(d)-LANL2DZ(Pt) level and given in Table 1. Considering Table 1, high-performance OLED consisting of the studied platinum(II) complexes can be designed. For example, Pt(fprpz)(fppz) and Pt(fprpz)(tbfppz) can be found in adjacent layers because their LUMO energy difference is .09 eV.

3.1.2 | Reorganization energies

Some OLED parameters of the mentioned complexes are calculated at the B3LYP/6-31G(d)-LANL2DZ(Pt) level in the Gaussian program and these values are presented in Table 1. It can be shown from data given in Table 1 that electron reorganization energies of the mentioned Pt(II)-complexes change from .18 to .39 eV. Considering the calculated electron reorganization energies, the λ_e values of all examined complexes except for Pt(f2bipz)(bpy) and Pt(mtpyim)(bipz) complexes are smaller than that of standard electron transport materials (ETL) which is AlQ3 ($\lambda_e = .276$) [96]. For this reason, one says that all complexes studied except for Pt(f2bipz)(bpy) and Pt(mtpyim)(bipz) compounds can be used as better ETL material than ALq3. Additionally, it is clear from Table 1 that the complexes with the lowest electron reorganization energy (.18 eV) are $Pt(hppz)_2$ and $Pt(fppz)_2$ molecules. Therefore, it can be indicated that $Pt(hppz)_2$ and $Pt(fppz)_2$ compounds can be utilized as the best candidates for ETL materials. Moreover, it is shown that the molecule having the highest electron reorganization energy (.39 eV) is Pt(f2bipz)(bpy). Thus, it can be stated that Pt(f2bipz)(bpy) can be suggested as an electron-blocking layer (EBL) material because of its high λ_e value [86].

From Table 1, it is seen that hole reorganization energies of the mentioned compounds vary from .31 to .62 eV. All hole reorganization energies obtained are higher than that of standard hole transport material (HTL) which is TPD ($\lambda_h = .290$) [97]. Therefore, it can be noted that all the complexes investigated are worse HTL candidates than TPD. However, it can be said that complexes 6 and 8 can be considered as hole-blocking layer (HBL) materials due to their high λ_h values [86].

As shown in Table 1, the compound having the lowest ionization and electron affinity potential is PtOEP compound. Thus, it can be said that PtOEP complex can be used as a good electron injection layer (EIL) material and a good hole injection layer (HIL) material [98]. In addition, when the chemical hardness values are examined from the same table, it is seen that the complex with the highest hardness value is Pt(fppz)(pic) complex. Accordingly, it can be said that the most stable complex among the studied platinum complexes is Pt(fppz)(pic) compound. In addition to these, Table 1 also shows that the dipole moments of $Pt(fprpz)_2$, $Pt(hppz)_2$, $Pt(fppz)_2$, and PtOEP compounds are zero or close to zero.

3.1.3 | NIR properties

In the Amsterdam DFT program, very costly energy calculations of the ground state (S0), the lowest energy singlet (S1) and the lowest energy triplet (T1) geometries of monomer complexes are made. After that, the energy differences between the mentioned states and the fluorescence or phosphorescence wavelengths corresponding to the differences are calculated. The obtained results are shown in Table 2. From Table 2, it is clear that the lowest energy emission value occurs in $Pt(hppz)_2$ compound. The emission color of this compound can be rudely predicted to be blue or close to blue. Additionally, it is clear from Table 2 that the compound with the highest emission wavelength is Pt(f2bipz)(bpy) complex. Considering the emission value of this complex, it can be stated that it is expected to be a good candidate for NIR-OLED because it has emission

TABLE 2 The energy differences (eV) between the ground (S0) and the singlet (S1) / the triplet (T1) states, the emission wavelengths (nm), spin-orbit matrix element (cm^{-1}), the rates of reverse intersystem crossing (s^{-1}) and intersystem crossing (s^{-1}) of the examined Pt(II)-complex monomers at 298.15 K.

Compound	S1–S0	T1–S0	S1–T1	Fl.	Ph.	SOCME $S_1 \leftrightarrow T_1$	K_{RISC} $T_1 \rightarrow S_1$	K_{ISC} $S_1 \rightarrow T_1$
$Pt(fprpz)_2$	2.78	2.51	.27	447	495	65.26	1.24×10^{15}	1.36×10^{20}
Pt(fprpz)(fppz)	2.85	2.54	.31	435	488	91.15	4.70×10^{14}	2.45×10^{20}
Pt(fprpz)(tbfppz)	2.83	2.44	.39	439	508	117.53	3.17×10^{13}	3.71×10^{20}
$Pt(hppz)_2$	3.13	2.81	.32	397	442	96.72	3.19×10^{14}	2.46×10^{20}
$Pt(fppz)_2$	3.11	2.79	.33	399	445	84.79	1.42×10^{14}	1.61×10^{20}
Pt(f2bipz)(bpy)	1.52	1.49	.03	813	831	.01	1.09×10^{9}	1.05×10^{10}
Pt(fppz)(pic)	2.95	2.77	.19	420	448	15.86	1.60×10^{15}	7.84×10^{18}
Pt(mtpyim)(bipz)	2.22	2.13	.09	558	581	11.02	3.60×10^{13}	3.58×10^{15}
1Pt	-	-	-	-	-	-	-	-
2Pt	-	-	-	-	-	-	-	-
PtOEP	2.64	2.02	.63	469	615	17.53	7.76×10^{-6}	1.04×10^{6}

wavelengths beyond 700 nm. Furthermore, it can be seen from the results given in the mentioned table that the triplet energies of 1Pt and 2Pt with open shell systems cannot be calculated. Therefore, the singlet-triplet transitions of the mentioned monomers could not be calculated.

3.1.4 | TADF performances

When the S1–T1 transition values, which determine the TADF OLED performance of the complexes, are examined in Table 2, it is seen that the S1–T1 values of Pt(f2bipz)(bpy), Pt(fppz)(pic) and Pt(mtpyim)(bipz) in the complexes examined are smaller than .2 eV. From these values, it can be noticed that these three complexes can be utilized as TADF OLED materials. From Table 2, it should be noted that Pt(f2bipz)(bpy) and Pt(mtpyim)(bipz) can be used as excellent TADF materials owing to their low S1–T1 value. Furthermore, it should be noted from results presented in Table 2 that Pt(f2bipz)(bpy) can be both a good TADF and a good NIR candidate.

To better interpret singlet-triplet transitions, the rates of reverse intersystem crossing (k_{RISC}) and the intersystem crossing (k_{ISC}) calculated 298.15 K with ΔE_{ST} and spin-orbit matrix element (SOCME) values are also reported in Table 2. Considering given data in Table 2, it is clear that intersystem crossing rates of $Pt(fprpz)_2$, Pt(fprpz)(fppz), Pt(fprpz)(tbfppz), $Pt(hppz)_2$, and $Pt(fppz)_2$ complexes are quite high ($\sim 10^{20}$ s^{-1}). From K_{ISC} values, one can say that $S_1 \rightarrow T_1$ intersystem crossing transitions of $Pt(fprpz)_2$, Pt(fprpz)(fppz), Pt(fprpz)(tbfppz), $Pt(hppz)_2$, and $Pt(fppz)_2$ will occur quite easily in the compounds studied. Referring to Table 2, it is seen that the rates of reverse intersystem crossing of the $Pt(fprpz)_2$ and Pt(fppz)(pic) compounds are quite high ($\sim 10^{15}$ s^{-1}) among the investigated complexes. From K_{RISC} values, it can be stated that $T_1 \rightarrow S_1$ reverse intersystem crossing transitions of $Pt(fprpz)_2$ and Pt(fppz)(pic) molecules can be quite easily in the examined Pt-complexes. Additionally, it can be said from given data in Table 2 that both K_{RISC} and K_{ISC} values of PtOEP complex is quite low among the studied molecules. Especially, it can be noted that T1-S1 reverse intersystem crossing transition of PtOEP compound is quite difficult.

Some quantum chemical descriptors calculated for the monomers in the Gaussian and ADF programs are calculated at the B3LYP/MIDIXL level in the Schrödinger program using the optimized structures obtained in the Gaussian program. In this way, the computational cost is greatly reduced. The results calculated are presented in Table 3. In this table, in addition to the data calculated in other programs, absorption values are also given. When Table 3 is compared with Tables 1 and 2, it is seen that the results calculated with different codes in different computational tools are largely compatible.

When Table 3 is compared with Table 1, it can be determined that reorganization energies and dipole moments calculated at B3LYP/6-31G(d)-LANL2DZ level are rather close to those of obtained at B3LYP/MIDIXL level. Additionally, it can be said that OLED parameters can be calculated more easily with the Schrödinger program using optimized geometries because the mentioned way has low computational cost. However, it can be noticed from Table 3 that reorganization energies and dipole moments of 1Pt and 2Pt complexes having open-shell systems cannot be calculated in Schrodinger program. It is required to note that it is easier to calculate the OLED parameters for molecules with a closed system with the Schrodinger program.

Another comparison is made to see whether the emission values in Table 3 are compatible with those in Table 2. For that reason, Emax values in Table 3 are compared with the emission wavelengths which are fluorescence and phosphorescence emission values in Table 2. It is seen that the wavelengths calculated at B3LYP/MIDIXL level in Table 3 is higher than those of PBE0/TZP level in Table 2. However, referring to both tables, a similar trend is observed for wavelengths. From Table 3 and Table 2, it is clear that the complex with the highest emission values is Pt(f2bipz)(bpy). As stated earlier, this compound is a good candidate for NIR OLED materials.

TABLE 3 The obtained reorganization energies (eV), absorption wavelengths (nm), emission wavelengths (nm), TADF parameters (eV), and dipole moments (Debye) of the investigated monomers at B3LYP/MIDIXL level.

Molecule	λe	λh	Lmax	Emax	S1-T1	Dipole
$Pt(fprpz)_2$	.22	.30	347	510	.42	.00
Pt(fprpz)(fppz)	.21	.30	336	503	.40	2.89
Pt(fprpz)(tbfppz)	.21	.30	334	505	.40	4.14
$Pt(hppz)_2$	.19	.33	322	453	.25	.02
$Pt(fppz)_2$	.17	.70	322	451	.41	.00
Pt(f2bipz)(bpy)	.37	.64	463	1000	.04	13.16
Pt(fppz)(pic)	.21	.42	329	557	.45	1.82
Pt(mtpyim)(bipz)	.99	.64	372	921	.07	14.82
1Pt	-	-	-	-	-	-
2Pt	-	-	-	-	-	-
PtOEP	.15	.33	463	579	.59	.32

Comparing Table 3 and Table 2 are compared in terms of TADF performances of molecules, it is shown that S1–T1 values in both the mentioned tables are quite compatible with each other. As shown in Table 3 and Table 2, one can say that Pt(f2bipz)(bpy) and Pt(mtpyim)(bipz) compounds can be an excellent candidate for TADF OLED materials because they have very low S1-T1 values.

Considering only Table 3, it is clearly seen that the Emax value of Pt(mtpyim)(bipz) are calculated as 921 nm. This value implies that Pt(mtpyim)(bipz) can be suggested as a good NIR OLED candidate such as Pt(f2bipz)(bpy).

3.2 | Dimers

Trans dimer structures of the mentioned Pt(II) complexes are optimized at PBE0/6-31G(d)-LANL2DZ(pt) level in the Gaussian program because previous works have shown that investigated complexes are stable in the trans form Reference [99]. Then obtained optimized dimers are included in the Schrödinger program. The geometries of the dimers taken from the Schrödinger program are shown in Figure 3. Some results of the dimers given in Figure 3 are achieved at the B3LYP/MIDIXL level in the Schrödinger program. As mentioned above, the computational cost is quite low in this way. The results obtained are given in Table 4. Apart from the aforementioned monomer calculations, Pt–Pt distances are also shown in the same table.

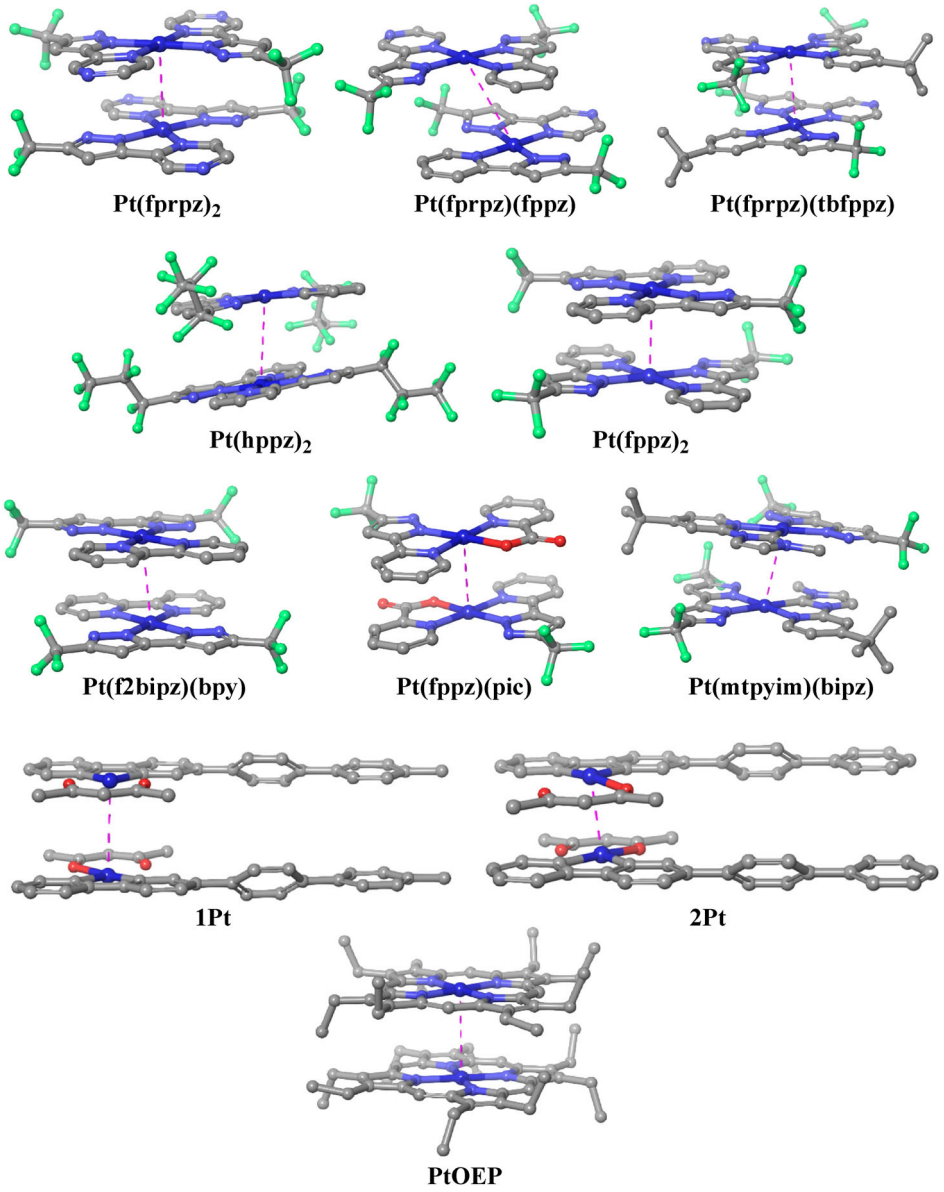

FIGURE 3 The optimized structures of the studied platinum(II)-complex dimers (H atoms are not shown.).

TABLE 4 The obtained reorganization energies (eV), the absorption wavelengths (nm), the emission wavelengths (nm), the TADF parameters (eV), the dipole moments (Debye), the Pt–Pt distances (Å) of the mentioned dimers at B3LYP/MIDIXL level.

Dimer	λe	λh	Lmax	Emax	S1-T1	Dipole	Pt-Pt distance
$Pt(fprpz)_2$	.18	.26	389	527	.17	.39	3.54
Pt(fprpz)(fppz)	.17	.29	416	501	.25	2.92	4.48
Pt(fprpz)(tbfppz)	.17	.17	414	502	.26	3.67	4.83
$Pt(hppz)_2$	.17	.18	393	446	.25	.61	4.56
$Pt(fppz)_2$	.16	.23	412	466	.20	.50	3.57
Pt(f2bipz)(bpy)	.42	.36	521	1000	.05	2.52	4.33
Pt(fppz)(pic)	.21	.26	401	527	.22	2.72	3.76
Pt(mtpyim)(bipz)	.21	.37	366	668	.10	7.70	4.12
1Pt	.72	.67	852	1000	.17	1.08	2.60
2Pt	.74	1.25	873	1000	.17	.16	2.60
PtOEP	.10	-	464	574	.58	.03	7.27

3.2.1 | Reorganization energies

The decrease of reorganization energies means the increase of OLED performance. As shown in Table 4, the dimerization, which occurs with the exception of Pt(f2bipz)(bpy), 1Pt, and 2Pt complexes generally reduces the reorganization energies. In addition, it should be noted from the same table that the 1Pt and 2Pt dimers are closed-shell since the 1Pt and 2Pt monomers have open-shell system form dimer. Therefore, it is seen that the OLED parameters of these dimers are also calculated in the Schrödinger program. Among the dimers, the best ETL candidate is PtOEP dimer. Additionally, one says that 1Pt and 2Pt dimers can be considered as good EBL materials because of their λ_e values. Although there are not a good HTL candidate in monomer complexes, all investigated dimers except for Pt(f2bipz)(bpy), Pt(mtpyim)(bipz), 1Pt and PtOEP dimers can be proposed as HTL candidates. Among these, it can be said that the best HTL compound is Pt(fprpz)(tbfppz) dimer. Furthermore, it can be said that Pt(fprpz)(tbfppz), $Pt(hppz)_2$, $Pt(fppz)_2$ and Pt(fppz)(pic) dimers which can be used as both ETL and HTL material is an ambipolar material. Finally, it can be stated that 2Pt dimer can be suggested as good HBL compound because of its high λ_h value.

3.2.2 | NIR properties

As seen in Table 4, the absorption values of the dimer complexes are usually higher than those of their monomers, whereas emission values of the dimers have not changed much compared with their monomers. From Table 4, it should be noted that emission values of the 2Pt and PtOEP dimers can be predicted as 1000 nm. Therefore, it can be indicated that these dimers can be suitable candidates as NIR OLED materials. Moreover, it may be seen from the same table that emission values of Pt(f2bipz)(bpy) dimer can be computed as 668 nm. This emission value is close to NIR region. For that reason, it can be suggested that Pt(f2bipz)(bpy) dimer may be NIR OLED candidate like its monomer.

3.2.3 | TADF performances

It is obviously seen from Table 4 that dimerization generally increases the TADF performance of the Pt(II) complexes. Among the investigated dimers, it can be said that $Pt(fprpz)_2$, Pt(f2bipz)(bpy), Pt(mtpyim)(bipz), 1Pt and 2Pt dimers can be considered as TADF OLED material because their S1-T1 values are smaller than .2 eV. Considering the TADF compounds, it can be easily said that the Pt(f2bipz)(bpy) dimer can be an excellent TADF material.

4 | CONCLUSIONS

Many OLED parameters of some platinum(II) monomers are estimated by Gaussian, ADF and Schrödinger programs. Within framework of the theoretically obtained results, suitable candidate(s) for all layers in OLED structure can be predicted. From the obtained reorganization values, it is apparent from the data presented in related table that $Pt(hppz)_2$ and $Pt(fppz)_2$ molecules can be used as ETL material. Furthermore, it should be

noted that Pt(f2bipz)(bpy) is both EBL and HBL materials. Additionally, it can be stated that PtOEP complex can be used as a good EIL and HIL material. Moreover, it is obvious from chemical hardness values shown in Table 1 that the most stable complex is Pt(fppz)(pic) compound among the investigated Pt(II)-complexes. On the other hand, it may be predicted from emission values and TADF parameters shown in related table that Pt(f2bipz)(bpy) molecule is a good candidate for NIR-OLED and TADF OLED.

Secondly, the OLED behaviors of the dimer form of the above complexes are estimated in a simple way by means of computational chemistry programs. From the obtained results, it should be noticed that dimerization of the Pt(II)-complexes generally increase their OLED performance. It is clear from data presented in Table 4 that reorganization energies of dimers are generally less than that of their monomers. Addition to this, it is clear from values presented in related to table that S1-T1 energy differences are also decreased with dimerization. Consequently, it should be noticed from the values given in related table that OLED performance of the examined Pt(II) complexes increase with dimerization. Finally, it should be noted that Pt(f2bipz)(bpy) dimer can used as a good NIR OLED material such us its monomer.

ACKNOWLEDGMENTS

The numerical calculations presented in this article were partially carried out at TUBITAK ULAKBIM, High Performance, and Grid Computing Center (TRUBA resources). In this study, the laboratory facilities of the Advanced Technology Application and Research Center of Sivas Cumhuriyet University (CÜTAM) were also used.

FUNDING INFORMATION

This work is supported by the Scientific Research Project Fund of Sivas Cumhuriyet University under the project numbers F-631.

CONFLICT OF INTEREST STATEMENT

The author declares no competing interests.

DATA AVAILABILITY STATEMENT

Data sharing not applicable to this article as no datasets were generated or analysed during the current study.

ORCID

Ayhan Üngördü https://orcid.org/0000-0002-7543-8379

REFERENCES

[1] C. W. Tang, S. A. VanSlyke, *Appl. Phys. Lett.* **1987**, *51*, 913.
[2] D. D. Zhang, L. Duan, *J. Phys. Chem. Lett.* **2019**, *10*, 2528.
[3] Shahnawaz, S. S. Swayamprabha, M. R. Nagar, R. A. K. Yadav, S. Gull, D. K. Dubey, J. H. Jou, *J. Mater. Chem. C* **2019**, *7*, 7144.
[4] D. D. Zhang, X. Z. Song, H. Y. Li, M. H. Cai, Z. Y. Bin, T. Y. Huang, L. Duan, *Adv. Mater.* **2018**, *30*, 30.
[5] C. T. Wang, C. C. Ting, P. C. Kao, S. R. Li, S. Y. Chu, *Appl. Phys. Lett.* **2018**, *113*, 113.
[6] N. Okamura, T. Nakamura, S. Yagi, T. Maeda, H. Nakazumi, H. Fujiwara, S. Koseki, *RSC Adv.* **2016**, *6*, 51435.
[7] J. Q. Shi, Z. Y. Ran, F. W. Peng, *Dyes Pigments* **2022**, *204*, 204.
[8] R. Sheng, L. P. Yang, A. S. Li, K. M. Chen, F. J. Zhang, Y. Duan, Y. Zhao, P. Chen, *J. Lumin.* **2022**, *246*, 246.
[9] Y. Liu, X. F. Tan, Q. Chen, L. Dai, W. P. Xiao, Y. P. Huo, *Chin. J. Liq. Cryst. Disp.* **2022**, *37*, 425.
[10] C. H. Chiu, N. R. Al Amin, J. X. Xie, C. C. Lee, D. Luo, S. Biring, K. Sutanto, S. W. Liu, C. H. Chen, *J. Mater. Chem. C* **2022**, *10*, 4955.
[11] L. Zhang, T. Ku, X. D. Cheng, Y. Song, D. Y. Zhang, *Microfluid. Nanofluid.* **2018**, *22*, 22.
[12] V. K. Chandra, B. P. Chandra, P. Jha, *Defect Diffus. Forum* **2014**, *357*, 29.
[13] A. Sure, K. R. Sarma, K. Paramanandam, R. H. Desai, A. Mukherjee, V. Baranwal, S. Asokan, *J. Disp. Technol.* **2015**, *11*, 1048.
[14] L. Zhao, H. Luo, P. Mei, J. A. Brug, F. Gomez-Pancorbo, E. Holland, W. Jackson, M. Jam, A. Jeans, J. Maltabes, C. M. Perlov, M. Smith, S. W. Trovinger, R. E. Elder, C. P. Taussig, R. Garcia, M. Almanza-Workman, H. J. Kim, O. Kwon, *Proc. China Disp./Asia Disp.* **2011**, *2011*, 112.
[15] B. X. Mi, H. S. Wang, Z. Q. Gao, X. P. Wang, R. F. Chen, W. Huang, *Prog. Chem.* **2011**, *23*, 136.
[16] Y. L. Liu, X. X. Man, Q. Bai, H. Liu, P. Y. Liu, Y. Fu, D. H. Hu, P. Lu, Y. G. Ma, *CCS Chem* **2022**, *4*, 214.
[17] Y. X. Zhang, J. Qiao, *Iscience* **2021**, *10*, 24.
[18] G. Q. Xia, C. Qu, Y. L. Zhu, K. Q. Ye, Z. L. Zhang, Y. Wang, *J. Mater. Chem. C* **2021**, *9*, 6834.
[19] C. Murawski, M. C. Gather, *Adv Opt Mater* **2021**, *9*, 9.
[20] R. He, Z. T. Xu, S. Valandro, H. D. Arman, J. G. Xue, K. S. Schanze, *ACS Appl. Mater. Interfaces* **2021**, *13*, 5327.
[21] Z. W. Hao, A. Ghanekarade, N. T. Zhu, K. Randazzo, D. Kawaguchi, K. Tanaka, X. P. Wang, D. S. Simmons, R. D. Priestley, B. Zuo, *Nature* **2021**, *596*, 372.
[22] H. Cho, C. W. Joo, S. Choi, C. M. Kang, G. H. Kim, J. W. Shin, B. H. Kwon, H. Lee, C. W. Byun, N. S. Cho, *ETRI J.* **2021**, *43*, 1093.
[23] C. Amruth, M. Pahlevani, G. C. Welch, *Mater Adv* **2021**, *2*, 628.
[24] A. K. Sajeev, N. Agarwal, A. Soman, S. Gupta, M. Katiyar, A. Ajayaghosh, K. N. N. Unni, *Org. Electron.* **2022**, *100*, 100.
[25] W. Chen, C. Xu, L. Kong, X. Y. Liu, X. Zhang, N. Lin, X. Ouyang, *Adv. Opt. Mater.* **2022**, *10*, 2102742.
[26] H. Y. Xiang, Y. Q. Li, S. S. Meng, C. S. Lee, L. S. Chen, J. X. Tang, *Adv. Opt. Mater.* **2018**, *6*, 6.
[27] L. H. Xu, Q. D. Ou, Y. Q. Li, Y. B. Zhang, X. D. Zhao, H. Y. Xiang, J. D. Chen, L. Zhou, S. T. Lee, J. X. Tang, *ACS Nano* **2016**, *10*, 1625.

[28] Y. L. Zhu, Y. Y. Hao, S. Q. Yuan, F. Zhang, Y. Q. Miao, Y. X. Cui, Z. F. Li, H. Wang, B. S. Xu, *Synth. Met.* **2015**, *203*, 200.
[29] C. H. Wang, C. C. Liu, *Comput. Ind. Eng.* **2022**, *169*, 108295.
[30] S. B. Li, L. Zhou, H. J. Zhang, *Light: Sci. Appl.* **2022**, *11*, 11.
[31] S. R. Forrest, *Nanophotonics* **2021**, *10*, 31.
[32] H. Okada, *2019 24th Microoptics Conference (Moc)*, IEEE, Toyama, Japan **2019**, p. 6.
[33] J. Wang, H. Pang, Z. Cui, X. Chen, R. Zheng, R. Kwong, S. Xia, *J. Soc. Inf. Disp.* **2022**, *6*, 495.
[34] X. Jiang, H. Lin, C. Xue, G. Zhang, W. Jiang, G. Xing, *J. Mater. Sci. Mater. Electron.* **2020**, *31*, 19136.
[35] H. Fujimoto, T. Nakamura, K. Nagayoshi, K. Harada, H. Miyazaki, T. Kurata, J. Kiyota, C. Adachi, *Appl. Phys. Lett.* **2020**, *116*, 143301.
[36] S. Negi, P. Mittal, B. Kumar, *Microsyst. Technol.* **2018**, *24*, 4981.
[37] Q. Wei, N. Fei, A. Islam, T. Lei, L. Hong, R. Peng, X. Fan, L. Chen, P. Gao, Z. Ge, *Adv Opt Mater* **2018**, *6*, 1800512.
[38] D. C. Santos, M. D. V. Marques, *J. Mater. Sci.: Mater. Electron.* **2022**, *33*, 12529.
[39] K. K. Kesavan, J. Jayakumar, M. Lee, H. Chen, S. S. Swayamprabha, D. K. Dubey, F. C. Tung, C. W. Wang, J. H. Jou, *Chem. Eng. J.* **2022**, *435*, 134879.
[40] Y. K. Qu, Q. Zheng, J. Fan, L. S. Liao, Z. Q. Jiang, *Acc. Mater. Res.* **2021**, *2*, 1261.
[41] C.-T. Chen, *Chem. Mater.* **2004**, *16*, 4389.
[42] Y. J. Pu, G. Nakata, F. Satoh, H. Sasabe, D. Yokoyama, J. Kido, *Adv. Mater.* **2012**, *24*, 1765.
[43] U. Tsiko, D. Volyniuk, V. Andruleviciene, K. Leitonas, G. Sych, O. Bezvikonnyi, V. Jasinskas, V. Gulbinas, P. Stakhira, J. V. Grazulevicius, *Mater Today Chem* **2022**, *25*, 25.
[44] L. Chen, S. Zhang, H. Li, R. Chen, L. Jin, K. Yuan, H. Li, P. Lu, B. Yang, W. Huang, *J. Phys. Chem. Lett* **2018**, *9*, 5240.
[45] D. L. Li, J. Y. Li, D. Liu, W. Li, C. L. Ko, W. Y. Hung, C. H. Duan, *ACS Appl. Mater. Interfaces* **2021**, *13*, 13459.
[46] M. Baldo, M. E. ThompSOn, S. Forrest, *Nature* **2000**, *403*, 750.
[47] W. Song, J. Y. Lee, *Adv Opt Mater* **2017**, *5*, 1600901.
[48] F. B. Dias, K. N. Bourdakos, V. Jankus, K. C. Moss, K. T. Kamtekar, V. Bhalla, J. Santos, M. R. Bryce, A. P. Monkman, *Adv. Mater.* **2013**, *25*, 3707.
[49] V. Jankus, P. Data, D. Graves, C. McGuinness, J. Santos, M. R. Bryce, F. B. Dias, A. P. Monkman, *Adv. Funct. Mater.* **2014**, *24*, 6178.
[50] C. Eickhoff, P. Murer, T. Gessner, J. Birnstock, M. Kroger, Z. S. Choi, S. Watanabe, F. May, C. Lennartz, I. Stengel, I. Munster, K. Kahle, G. Wagenblast, H. Mangold, *Org. Light-Emitting Mater. Devices* **2015**, *19*, 9566.
[51] V. V. Patil, H. Lee, I. Kim, K. H. Lee, W. J. Chung, J. Kim, S. Park, H. Choi, W. J. Son, S. O. Jeon, J. Y. Lee, *Adv. Sci.* **2021**, *8*, 8.
[52] H. Z. Li, D. Zhang, F. M. Xie, X. Y. Zeng, Y. Q. Li, H. X. Wei, G. L. Dai, J. X. Tang, X. Zhao, *Dyes Pigments* **2021**, *188*, 188.
[53] Y.-W. Chen, C.-C. Tsai, H.-Y. Chih, H.-Y. Tsai, W.-Y. Wang, G.-Y. Liu, M.-Y. Wu, C.-H. Chang, C.-W. Lu, *Dyes Pigments* **2022**, *197*, 109892.
[54] Y. Xia, Z. M. Liu, J. Li, C. C. Fan, G. Li, B. Zhao, Y. L. Wu, H. Wang, K. P. Guo, *Org. Electron.* **2020**, *85*, 85.
[55] M. T. Sharbati, F. Panahi, A. Gharavi, *IEEE Photonics Technol. Lett* **2010**, *22*, 1695.
[56] Y. J. Yu, Y. Hu, S. Y. Yang, W. Luo, Y. Yuan, C. C. Peng, J. F. Liu, A. Khan, Z. Q. Jiang, L. S. Liao, *Angew. Chem. Int. Edit.* **2020**, *59*, 21578.
[57] A. Zampetti, A. Minotto, F. Cacialli, *Adv. Funct. Mater.* **2019**, *29*, 29.
[58] J. X. Jiang, Z. Xu, J. D. Zhou, M. Hanif, Q. L. Jiang, D. H. Hu, R. Y. Zhao, C. Wang, L. L. Liu, D. G. Ma, Y. G. Ma, Y. Cao, *Chem. Mater.* **2019**, *31*, 6499.
[59] Z. L. Zhu, J. H. Tan, W. C. Chen, Y. Yuan, L. W. Fu, C. Cao, C. J. You, S. F. Ni, Y. Chi, C. S. Lee, *Adv. Funct. Mater.* **2021**, *31*, 2102787.
[60] L. Y. Cao, J. J. Li, Z. Q. Zhu, L. Huang, J. Li, *ACS Appl. Mater. Interfaces* **2021**, *13*, 60261.
[61] A. Zampetti, A. Minotto, F. Cacialli, *Adv. Funct. Mater.* **2019**, *29*, 1807623.
[62] G. Cheng, Q. Wan, W. H. Ang, C. L. Kwong, W. P. To, P. K. Chow, C. C. Kwok, C. M. Che, *Adv Opt Mater* **2019**, *7*, 1801452.
[63] M. Sassi, N. Buccheri, M. Rooney, C. Botta, F. Bruni, U. Giovanella, S. Brovelli, L. Beverina, *Sci. Rep.* **2016**, *6*, 1.
[64] L. Tu, Y. Xie, Z. Li, B. Tang, *SmartMat* **2021**, *2*, 326.
[65] Y.-C. Wei, S. F. Wang, Y. Hu, L.-S. Liao, D.-G. Chen, K.-H. Chang, C.-W. Wang, S.-H. Liu, W.-H. Chan, J.-L. Liao, *Nat. Photonics* **2020**, *14*, 570.
[66] M. Ibrahim-Ouali, F. Dumur, *Molecules* **2019**, *24*, 1412.
[67] C. C. Tong, K. C. Hwang, *J. Phys. Chem. C* **2007**, *111*, 3490.
[68] G. Hong, X. Gan, C. Leonhardt, Z. Zhang, J. Seibert, J. M. Busch, S. Bräse, *Adv. Mater.* **2021**, *33*, 2005630.
[69] G. Mancino, A. J. Ferguson, A. Beeby, N. J. Long, T. S. Jones, *J. Am. Chem. Soc.* **2005**, *127*, 524.
[70] C. Doffek, N. Alzakhem, M. Molon, M. Seitz, *Inorg. Chem.* **2012**, *51*, 4539.
[71] B. L. Reid, S. Stagni, J. M. Malicka, M. Cocchi, A. N. Sobolev, B. W. Skelton, E. G. Moore, G. S. Hanan, M. I. Ogden, M. Massi, *Chem Eur J* **2015**, *21*, 18354.
[72] Y. Zhang, D. Zhang, T. Huang, A. J. Gillett, Y. Liu, D. Hu, L. Cui, Z. Bin, G. Li, J. Wei, *Angew. Chem. Int. Ed.* **2021**, *60*, 20498.
[73] Y. Shen, Z. Zhang, H. Liu, Y. Yan, S. Zhang, B. Yang, Y. Ma, *J. Phys. Chem. C* **2019**, *123*, 13047.
[74] A. Minotto, I. Bulut, A. G. Rapidis, G. Carnicella, M. Patrini, E. Lunedei, H. L. Anderson, F. Cacialli, *Light: Sci. Appl.* **2021**, *10*, 1.
[75] E. A. Wood, L. F. Gildea, D. S. Yufit, J. G. Williams, *Polyhedron* **2021**, *207*, 115401.
[76] A. Heil, C. M. Marian, *Inorg. Chem.* **2019**, *58*, 6123.
[77] M. R. Prabhath, J. Romanova, R. J. Curry, S. R. P. Silva, P. D. Jarowski, *Angew. Chem. Int. Ed.* **2015**, *54*, 7949.
[78] K. Li, G. S. M. Tong, Q. Wan, G. Cheng, W.-Y. Tong, W.-H. Ang, W.-L. Kwong, C.-M. Che, *Chem. Sci.* **2016**, *7*, 1653.
[79] K. H. Kim, J. J. Kim, *Adv. Mater.* **2018**, *30*, 1705600.
[80] M. J. Frisch, G. W. Trucks, H. B. Schlegel, G. E. Scuseria, M. A. Robb, J. R. Cheeseman, G. Scalmani, V. Barone, G. A. Petersson, H. Nakatsuji, X. Li, M. Caricato, A. V. Marenich, J. Bloino, B. G. Janesko, R. Gomperts, B. Mennucci, H. P. Hratchian, J. V. Ortiz, A. F. Izmaylov, J. L. Sonnenberg, Williams, F. Ding, F. Lipparini, F. Egidi, J. Goings, B. Peng, A. Petrone, T. Henderson, D. Ranasinghe, V. G. Zakrzewski, J. Gao, N. Rega, G. Zheng, W. Liang, M. Hada, M. Ehara, K. Toyota, R. Fukuda, J. Hasegawa, M. Ishida, T. Nakajima, Y. Honda, O. Kitao, H. Nakai, T. Vreven, K. Throssell, J. A. Montgomery Jr., J. E. Peralta, F. Ogliaro, M. J. Bearpark, J. J. Heyd, E. N. Brothers, K. N. Kudin, V. N. Staroverov, T. A. Keith, R. Kobayashi, J. Normand, K. Raghavachari, A. P. Rendell, J. C. Burant, S. S. Iyengar, J. Tomasi, M. Cossi, J. M. Millam, M. Klene, C. Adamo, R. Cammi, J. W. Ochterski, R. L. Martin, K. Morokuma, O. Farkas, J. B. Foresman, D. J. Fox, Wallingford, CT. **2016**.
[81] G. te Velde, F. M. Bickelhaupt, E. J. Baerends, C. F. Guerra, S. J. A. Van Gisbergen, J. G. Snijders, T. Ziegler, *J. Comput. Chem.* **2001**, *22*, 931.
[82] A. D. Bochevarov, E. Harder, T. F. Hughes, J. R. Greenwood, D. A. Braden, D. M. Philipp, D. Rinaldo, M. D. Halls, J. Zhang, R. A. Friesner, *Int. J. Quantum Chem.* **2013**, *113*, 2110.

[83] M. N. Arshad, I. Shafiq, M. Khalid, A. M. Asiri, *ACS Omega* **2022**, *7*, 11606.
[84] X. Li, B. Minaev, H. Ågren, H. Tian, *J. Phys. Chem. C* **2011**, *115*, 20724.
[85] R. A. Marcus, *Rev. Mod. Phys.* **1993**, *65*, 599.
[86] U. Daswani, U. Singh, P. Sharma, A. Kumar, *J. Phys. Chem. C* **2018**, *122*, 14390.
[87] S. S. Tang, J. P. Zhang, *J. Phys. Chem. A* **2011**, *115*, 5184.
[88] A. Irfan, A. Kalam, A. R. Chaudhry, A. G. Al-Sehemi, S. Muhammad, *Optik* **2017**, *132*, 101.
[89] R. G. Pearson, *J. Am. Chem. Soc.* **1988**, *110*, 7684.
[90] Y. Tao, K. Yuan, T. Chen, P. Xu, H. Li, R. Chen, C. Zheng, L. Zhang, W. Huang, *Adv. Mater.* **2014**, *26*, 7931.
[91] V. Lawetz, G. Orlandi, W. Siebrand, *J. Chem. Phys.* **1972**, *56*, 4058.
[92] G. W. Robinson, R. Frosch, *J. Chem. Phys.* **1963**, *38*, 1187.
[93] C. L. Kim, J. Jeong, H. J. Jang, K. H. Lee, S.-T. Kim, M.-H. Baik, J. Y. Lee, *J. Mater. Chem. C* **2021**, *9*, 8233.
[94] Y. Ohtomo, K. Ishiwata, S. Hashimoto, T. Kuroiwa, K. Tahara, *J. Org. Chem.* **2021**, *86*, 13198.
[95] R. A. K. Yadav, D. K. Dubey, S.-Z. Chen, T.-W. Liang, J.-H. Jou, *Sci. Rep.* **2020**, *10*, 1.
[96] A. Lukyanov, C. Lennartz, D. Andrienko, *Phys. Status Solidi A* **2009**, *206*, 2737.
[97] N. E. Gruhn, D. A. da Silva Filho, T. G. Bill, M. Malagoli, V. Coropceanu, A. Kahn, J.-L. Brédas, *J. Am. Chem. Soc.* **2002**, *124*, 7918.
[98] A. A. Youssef, S. M. Bouzzine, Z. M. E. Fahim, İ. Sıdır, M. Hamidi, M. Bouachrine, *Phys. B* **2019**, *560*, 111.
[99] Y. Chi, H. Y. Tsai, Y. K. Chen, *J Chin Chem Soc* **2017**, *64*, 574.

How to cite this article: A. Üngördü, *Int. J. Quantum Chem.* **2023**, *123*(21), e27208. https://doi.org/10.1002/qua.27208